Interfacial Phenomena and Heat Transfer, 5(4):287–298 (2017)

SIDEBAND THERMOCAPILLARY INSTABILITY OF A THIN FILM COATING THE OUTSIDE OF A THICK WALLED CYLINDER WITH FINITE THERMAL CONDUCTIVITY IN THE ABSENCE OF GRAVITY

Luis Antonio Dávalos-Orozco

Instituto de Investigaciones en Materiales, Departamento de Polímeros, Universidad Nacional Autónoma de México, Ciudad Universitaria, Circuito Exterior S/N, Delegación Coyoacán, 04510 México D.F., México; Tel.: +55 556 224 601; Fax: +55 556 161 201, E-mail: ldavalos@unam.mx

Original Manuscript Submitted: 11/8/2017; Final Draft Received: 2/27/2018

The sideband thermocapillary instability of a thin liquid film coating the outside of a heated cylinder in the absence of gravity is investigated. Previous results show that, for a Newtonian fluid and under the approximation of small wave number and large radius of the cylinder, the axial and all azimuthal modes with wave number $k_{max} > 0$ have the same linear maximum growth rate. Therefore, it is our goal to solve this linear indeterminacy from the nonlinear point of view and find the parameter regions where the axial mode and the first azimuthal mode may prevail.

KEY WORDS: *cylindrical thin liquid film, Marangoni convection, thermocapillary convection, nonlinear sideband instability, thick wall, wall finite thermal conductivity*

1. INTRODUCTION

The coating of surfaces is important in industrial applications. In particular, the coating of cylinders and wires has its own problems due to different instabilities that may occur in the process. Therefore, it is of interest to understand flow behavior after a perturbation is applied to the liquid or directly at the free surface. The perturbations can be isothermal and nonisothermal. The second one corresponds to Marangoni thermocapillary instability.

The stability of thin films flowing down a cylinder has been investigated theoretically by a number of authors. In particular, in the small wave number, large cylinder radius, and very strong surface tension approximation, a model equation was obtained by Shlang and Sivashinsky (1982). That evolution equation included the azimuthal effects in the free surface perturbations. The flow inside a cylinder is also of interest. The two-layer flow inside a capillary tube was investigated by Frenkel et al. (1987). Frenkel (1993) relaxed the condition of very strong surface tension of Shlang and Sivashinsky (1982) to obtain an evolution equation of the Benney type (Benney, 1996) but including azimuthal perturbations. By means of the linear versions of both equations (Shlang and Sivashinsky, 1982; Frenkel, 1993) it is possible to show that, under their particular approximations, the azimuthal modes are able to appear but the axial mode ($m = 0$) is always the most unstable one. The linear instability of the flow down the inside and the outside of a rotating cylinder has been investigated analytically in the small wave number approximation by Dávalos-Orozco and Ruiz-Chavarría (1993), in the small Reynolds number approximation by Ruiz-Chavarría and Dávalos-Orozco (1996), and numerically in Ruiz-Chavarría and Dávalos-Orozco (1997). It is shown that for certain magnitudes of the Reynolds number and of the rotation parameter it is possible to find the first azimuthal mode (m = 1) as the most unstable one. The instability of the flow of a viscoelastic fluid down a cylinder was investigated by Moctezuma-Sánchez and Dávalos-Orozco (2008). It is found that viscoelasticity excites the appearance of azimuthal modes in comparison to flow in a Newtonian fluid, but the axial mode ($m = 0$) remains as the most unstable one.

2169–2785/17/$35.00

NOMENCLATURE

a	radius δ scaled with ξ
A	time-dependent complex amplitudes of the normal modes
A_c	time-dependent complex conjugate amplitudes of the normal modes
Bi	free surface–atmosphere Biot number
c	phase velocity
c_1	phase velocity to ride on the wave
Cr	Crispation number
Cr_{min}	Crispation number of the minimum of the maximum growth rate
d	relative thickness of the wall
den	$= 1 + \mathrm{Bi}(1 + d/Q_C)$
h	free surface deformation
h_0	mean thickness of the layer
H	free surface perturbation amplitude
H_0	constant free surface amplitude
H_h	heat transfer coefficient
H_n	amplitudes of free surface expansion
J	Jacobian matrix
k	axial wave number
k_C	critical wave number
k_{max}	maximum growth rate wave number
m	azimuthal number
Ma	Marangoni number
Q_C	wall to liquid thermal conductivities ratio
R	cylinder radius
$S(\mathrm{Bi}, d/Q_C)$	$= 1 - \mathrm{Bi}/den$
$\overline{T}$	temperature

Greek Symbols

α	fluid thermal diffusivity
β	nondimensional cylinder radius
γ	surface tension
δ	scaled nondimensional radius
ΔT	temperature difference
ε	smallness parameter
θ	azimuthal angle
λ	coefficients of normal modes equations
μ	stability parameter of nonlinear problem
ν	kinematic viscosity
ξ	scaling parameter $\sqrt{\mathrm{Cr}}$
ρ	fluid density
σ	growth rate
σ_{max}	maximum growth rate for $k_{max} > 0$
$\sigma_{max\,k=0}$	maximum growth rate at k = 0
$\sigma_{max-min}$	minimum of the maximum growth rate with Cr_{min}
ω	frequency of oscillation

The effect of thermocapillarity in the absence of gravity was investigated by Dijkstra (1990). By means of numerical analysis of the linear equations of motion and heat transfer he found that by means of the thermal Marangoni effect it is possible to find azimuthal modes as the most unstable ones for different regions of the wave number k, in particular when the wave number is $k = 0$. The linear Marangoni instability of a thin film flowing down a hot cylinder was investigated by Dávalos-Orozco and You (2000). They studied the instability inside and outside of the cylinder in the absence and in the presence of gravity. It is found in the absence of gravity that modes up to $m = 13$ can be excited as the most unstable outside the cylinder for $k \to 0$. In the presence of gravity, the results show that very high azimuthal modes can be excited as the most unstable for small Reynolds numbers and wave numbers. In both cases the azimuthal modes are easier to excite with the increase of the radius of the cylinder. More recently, Moctezuma-Sánchez and Dávalos-Orozco (2015) made calculations on the thermocapillary instability of a viscoelastic liquid flowing down a cylinder. The instability in the absence of gravity was also investigated. It is found that viscoelastic and thermocapillary effects stimulate the appearance of azimuthal modes, but the axial mode always has the maximum growth rate.

When making numerical calculations of the Orr-Sommerfeld equation for the linear stability (Dijkstra, 1990; Dávalos-Orozco and You, 2000), the range of the parameters investigated gives a good idea of the flow behavior.

However, when analytical approximations are done, it is possible to look with more detail at particular regions of the parameters' space. In Moctezuma-Sánchez and Dávalos-Orozco (2015) calculations were done for small wave number and large radius of the cylinder, following the approximations by Frenkel (1993). Nevertheless, it was surprising that the linear analytical results in Moctezuma-Sánchez and Dávalos-Orozco (2015) show that in the absence of viscoelasticity and gravity, the maximum growth rate of a Newtonian fluid is the same for the axial mode and all azimuthal modes when the corresponding wave number k_{max} is different from zero. Notice that this does not occur when the maximum growth rate is located at $k_{max\,k=0} = 0$. However, observe that the absolute maximum occurs only when $k_{max} > 0$. That is, $k_{max} > k_{max\,k=0}$, always. It is concluded that it is not possible, from the linear point of view, to determine which mode will be the most unstable one when $k_{max} > 0$.

The goal of the present paper is to give a solution to this linear indeterminacy found in Moctezuma-Sánchez and Dávalos-Orozco (2015) in the absence of viscoelasticity by means of nonlinear analytical calculations of the thermocapillary sideband instability of the axial mode against the first azimuthal mode. To attain this goal the nonlinear evolution equation of the present problem is investigated using the theory of Cheng and Chang (1992). This is the first time those calculations are applied to a thermocapillary problem outside a cylinder.

It is important to point out that in Ruiz-Chavarría and Dávalos-Orozco (1997), numerical analysis was done of the full generalized set of two coupled linear Orr-Sommerfeld equations for flow down a rotating cylinder. However, in the absence of gravity, the cylinder is not under rotation, and the film is heated from the wall of the cylinder. More important is that here use is made of the small wave number and large radius of the cylinder approximations. The present paper is more intimately related with that of Moctezuma-Sánchez and Dávalos-Orozco (2015).

The structure of the paper is as follows: the evolution equation calculated under the small wave number and large radius of the cylinder approximation (Frenkel, 1993) in the absence of gravity is presented in the next section. There, the results of the linear growth rate and maximum growth rate are also discussed. The evolution equation is further approximated to very strong surface tension in Section 3. The sideband instability is investigated from the resulting evolution equation. The conclusions are given in Section 4.

2. EVOLUTION EQUATION

A Newtonian liquid thin film is coating the outside of a circular cylinder with a thick wall of finite thermal conductivity. The temperature inside the cylinder is higher than that of the atmosphere (see Fig. 1). In this case, thermocapillary convection occurs when the temperature gradient across the wall and the film attains a magnitude large enough that surface tension variations with temperature are able to overcome viscose effects to start the motion of the liquid film. The free surface of the film is deformable and its distortion can be described by means of an approximate nonlinear evolution equation. This equation is calculated following Frenkel (1993). However, in the absence of gravity there is no main flow in the axial direction ($w_0 = 0$) and the velocity components have to be expanded as

$$u = \varepsilon^2(u_0 + \varepsilon u_1 + \cdots), \quad v = \varepsilon(v_0 + \varepsilon v_1 + \cdots), \quad w = \varepsilon(w_1 + \varepsilon w_2 \cdots), \tag{1}$$

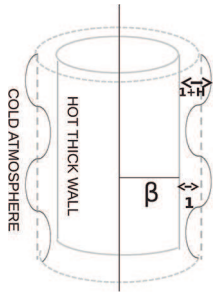

FIG. 1: Heated liquid film coating the outside of cylinder with a thick wall in the absence of gravity. The nondimensional thickness of the film is 1 and H is the perturbation. β is the nondimensional radius of the cylinder

where (u, v, w) are the velocity components in the radial, azimuthal, and axial directions, respectively. The other variables are expanded in the same way as in Moctezuma-Sánchez and Dávalos-Orozco (2015). The nonlinear evolution equation is

$$h_t + \frac{1}{3\text{Cr}}\nabla_\perp \cdot \left[h^3 \nabla_\perp \left(\frac{1}{\delta^2}h + \nabla_\perp^2 h\right)\right] + \frac{1}{2}\text{MaBi}\nabla_\perp \cdot \left\{\frac{h^2}{\left[1 + \text{Bi}h + \text{Bi}(d/Q_C)\right]^2}\nabla_\perp h\right\} = 0. \tag{2}$$

The relative thickness of the wall d is defined as the ratio of the thickness of the wall divided by thickness of the unperturbed flat liquid film h_0. The ratio of the wall thermal conductivity over that of the liquid layer is Q_C. Notice that when linearizing, this [Eq. (2)] reduces to that calculated by Moctezuma-Sánchez and Dávalos-Orozco (2015) in the absence of viscoelasticity and for d = 0. Besides, the equation reduces to the nonlinear Eq. 1 of Krishnamoorthy et al. (1995) in the absence of gravity (their G = 0), d = 0 (or else, $Q_C \to \infty$) and $\delta \to \infty$ (very large relative radius of the cylinder). In the last step it is important to assume y = δθ as finite to preserve the operator $\nabla_\perp$ defined as

$$\nabla_\perp = \left(\frac{\partial}{\partial z}, \frac{1}{\delta}\frac{\partial}{\partial \theta}\right). \tag{3}$$

The nondimensional radius of the cylinder is defined as $\beta = R/h_0$. The scaled radius of the cylinder is $\delta = \varepsilon\beta$. This scaling is needed under the assumption of a very large radius of the cylinder. $\varepsilon < 1$ is a smallness parameter which is the ratio of the representative thickness of the liquid film h_0 divided by the representative wavelength of the free surface perturbations. It is important to point out that the relative thickness of the wall d cannot be larger than the nondimensional radius of the cylinder β. The reason is that when $d < \beta$ the cylinder is a tube with a thick wall and with a void nucleus (possibly filled with hot air). When $d = \beta$ the cylinder is already a solid bar without a void nucleus. Larger values of d are unphysical.

The total height of the free surface deformation is $h(z, \theta, t)$. Here z is the axial coordinate and θ is the azimuthal angle. The crispation number is Cr = $\rho\alpha\nu/\gamma h_0$, the Marangoni number is Ma = $-(d\gamma/d\overline{T})\Delta T h_0/\rho\alpha\nu$, and the Biot number is Bi = $H_h/k_f h_0$. ΔT is the difference between the temperature of the inner side of the wall and that of the atmosphere outside the liquid film. The liquid film has density ρ, kinematic viscosity ν, thermal conductivity α, a surface tension γ, and surface heat transfer coefficient H_h. Notice that the ratio d/Q_C in Eq. (2) has been obtained following Dávalos-Orozco (2012, 2014, 2015, 2016). In this sense, it is the first time Eq. (2) has been calculated including the effects of thermal conductivity and thickness of the wall. Then, the results presented below are new for the thermocapillary instability in the outer surface of a cylinder.

Equation (2) can be linearized assuming normal modes in the form $h(z, \theta, t) = 1 + H_0 \exp[i(kz + m\theta + \omega t) + \sigma t]$, where H_0 is the amplitude of the perturbation, k is the axial wave number, m is the azimuthal integer number, ω is the frequency of oscillation, and σ is the growth rate. After substitution, the imaginary part corresponds to the frequency of oscillation from which the phase velocity is

$$c = \frac{\omega}{k} = 0, \tag{4}$$

and the flow is stationary. The real part corresponds to the growth rate

$$\sigma = -\frac{k^4}{3\text{Cr}} + \left\{\frac{1 - 2m^2}{3\text{Cr}\delta^2} + \frac{1}{2}\frac{\text{MaBi}}{\left[1 + \text{Bi} + \text{Bi}(d/Q_C)\right]^2}\right\}k^2 + \frac{m^2\left(1 - m^2\right)}{3\text{Cr}\delta^4} + \frac{m^2}{2\delta^2}\frac{\text{MaBi}}{\left[1 + \text{Bi} + \text{Bi}(d/Q_C)\right]^2}, \tag{5}$$

The critical wave number is obtained when the growth rate is zero. That is

$$k_C = \left\{\frac{1 - 2m^2}{\delta^2} + \frac{3}{2}\text{Cr}\frac{\text{MaBi}}{\left[1 + \text{Bi} + \text{Bi}(d/Q_C)\right]^2}\right\}^{1/2}. \tag{6}$$

The maximum growth rate is calculated taking the k derivative of σ in Eq. (5). Two maxima appear for two magnitudes of the wave number. For a zero wave number k_{max} = 0 the maximum is

$$\sigma_{max\,k=0} = -\frac{m^4}{2\text{Cr}\delta^4} + \frac{m^2}{\delta^2}\left\{\frac{1}{3\text{Cr}\delta^2} + \frac{1}{2}\frac{\text{MaBi}}{\left[1 + \text{Bi} + \text{Bi}(d/Q_C)\right]^2}\right\}. \tag{7}$$

When the wave number of the maximum is different from zero the magnitude is

$$k_{max} = \frac{1}{\sqrt{2}} \left\{ \frac{1-2m^2}{\delta^2} + \frac{3}{2}\mathrm{Cr}\frac{\mathrm{MaBi}}{\left[1+\mathrm{Bi}+\mathrm{Bi}(d/Q_C)\right]^2} \right\}^{1/2}. \tag{8}$$

Notice that $k_{max} \neq 1/\sqrt{2}\ k_C$. The equality holds in two cases. The first one is when the problem is one-dimensional, $m = 0$, that is, in the absence of azimuthal modes. The second one is when the wall surface is flat, that is, when $\delta \to \infty$ (see Dávalos-Orozco, 2012, 2014, 2015, 2016). Substitution of Eq. (8) into Eq. (5) leads to

$$\sigma_{max} = \frac{1}{3\mathrm{Cr}} \left\{ \frac{1-2m^2}{2\delta^2} + \frac{3}{4}\mathrm{Cr}\frac{\mathrm{MaBi}}{\left[1+\mathrm{Bi}+\mathrm{Bi}(d/Q_C)\right]^2} \right\}^2 + \frac{m^2\left(1-m^2\right)}{3\mathrm{Cr}\delta^4} + \frac{m^2}{2\delta^2}\frac{\mathrm{MaBi}}{\left[1+\mathrm{Bi}+\mathrm{Bi}(d/Q_C)\right]^2}, \tag{9}$$

where it can be seen that the first two terms of Eq. (5) can be cast into a squared binomial. Apparently σ_{max} for $k_{max} > 0$ differs for different azimuthal modes m. However, Eq. (9) is misleading because expanding the binomial and simplifying, it is found that

$$\sigma_{max} = \frac{3}{4}\mathrm{Cr}\left\{ \frac{1}{3\mathrm{Cr}\delta^2} + \frac{1}{2}\frac{\mathrm{MaBi}}{\left[1+\mathrm{Bi}+\mathrm{Bi}(d/Q_C)\right]^2} \right\}^2 \tag{10}$$

is independent of the azimuthal mode m. The axial and all azimuthal modes$m$with $k_{max} > 0$ have the same maximum growth rate. Therefore, it is not possible to determine from the linear point of view which mode will prevail. Notice that $\sigma_{max} > \sigma_{max\,k=0}$, always. Then, in the nonlinear calculations of the next section, the problem is only devoted to the case $k_{max} > 0$.

The behavior of the growth rate Eq. (5) for different magnitudes of the parameters d/Q_C, δ, Cr, and Ma are described in Figs. 2–5. The Biot number is fixed at Bi = 0.1. Figure 2 displays results for a radius δ = 5 and d/Q_C = 1. The influence of the Marangoni number on the growth rate is apparent in Figs. 2(a)–2(c). Each figure presents curves for different Cr, which has no monotonic influence on the instability. Notice that the ratio d/Q_C is the important one, and not each of its components. Besides, note that an increase of Crrepresents a decrease of surface tension. It is also shown that an increase of Ma excites the appearance of azimuthal modes. However, the increase of d/Q_C works against this behavior as can be seen in Fig. 3 for d/Q_C = 5 by comparison of Figs. 3(a)–3(c) with their corresponding Figs. 2(a)–2(c). The maximum growth rate decreases.

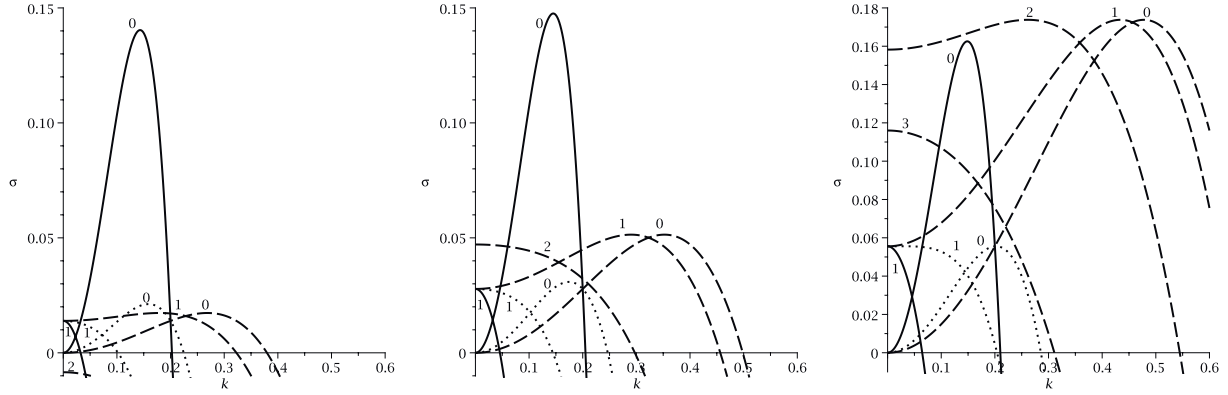

FIG. 2: σ vs. k; Bi = 0.1 and δ = 5; d/Q_C = 1. (a) Ma = 10, (b) Ma = 20, (c) Ma = 40. Solid Cr = 0.001, dotted Cr = 0.01, dashed Cr = 0.1; m = 0, 1, 2, 3

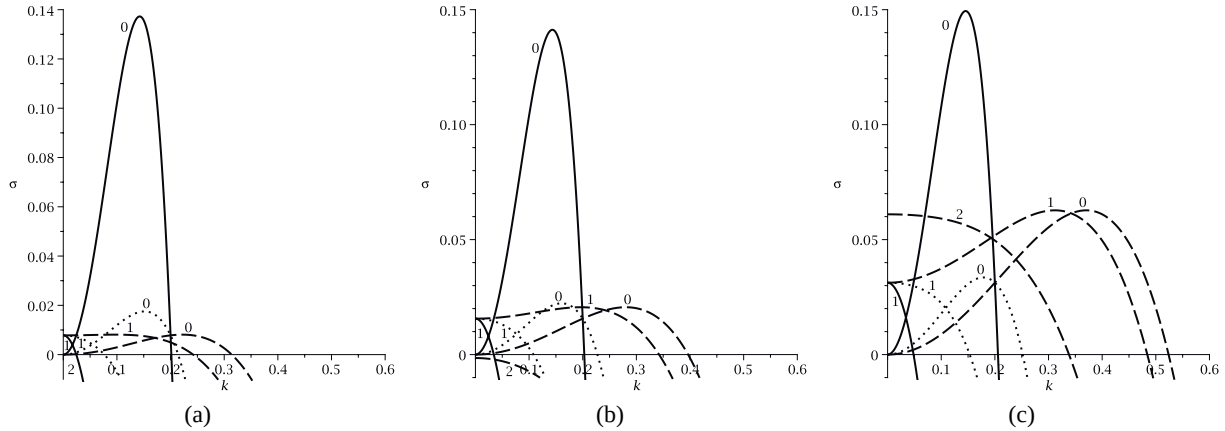

FIG. 3: σ vs. k; Bi = 0.1 and δ = 5; d/Q_C = 5. (a) Ma = 10, (b) Ma = 20, (c) Ma = 40. Solid Cr = 0.001, dotted Cr = 0.01, dashed Cr = 0.1; m = 0, 1, 2, 3

A large radius of the cylinder stimulates the appearance of azimuthal modes in the region $k > 0$. This is shown in Fig. 4 where δ = 10 and d/Q_C = 1. In this case, the growth rate increases notably with the increase of Ma. This effect is diluted in case the ratio increases to d/Q_C = 5 as in Fig. 5. However, the Marangoni number still stimulates the growth of the azimuthal modes as shown in Figs. 5(a)–5(c).

In general, in Figs. 2–5, the maximum of the axial mode $m = 0$ is always located at a wave number to the right of that corresponding to the first azimuthal mode $m = 1$. The wave numbers of the maxima of higher azimuthal modes are displaced to the left with respect to that of $m = 1$. It is important to point out that the increase of surface tension from Cr = 0.1 to 0.001 does not produce a monotonic increase of the maximum growth rate, Eq. (10), as it is confirmed in Figs. 2–5. In fact, it has a minimum at

$$\mathrm{Cr}_{min} = 1/\left(3\delta^2\left\{\frac{1}{2}\frac{\mathrm{MaBi}}{\left[1+\mathrm{Bi}+\mathrm{Bi}(d/Q_C)\right]^2}\right\}\right) \quad \text{and} \quad \sigma_{max-min} = \frac{1}{2\delta^2}\frac{\mathrm{MaBi}}{\left[1+\mathrm{Bi}+\mathrm{Bi}(d/Q_C)\right]^2}. \tag{11}$$

In Fig. 3(a), a monotonic behavior can be seen. The reason is that the corresponding parameters set locates σ_{max} far from the minimum.

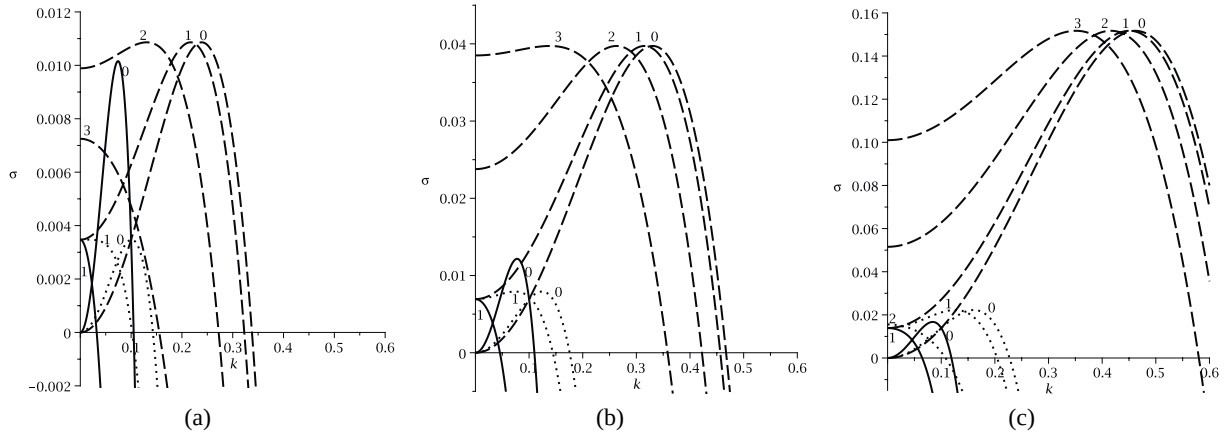

FIG. 4: σ vs. k; Bi = 0.1 and δ = 10; d/Q_C = 1. (a) Ma = 10, (b) Ma = 20, (c) Ma = 40. Solid Cr = 0.001, dotted Cr = 0.01, dashed Cr = 0.1; m = 0, 1, 2, 3

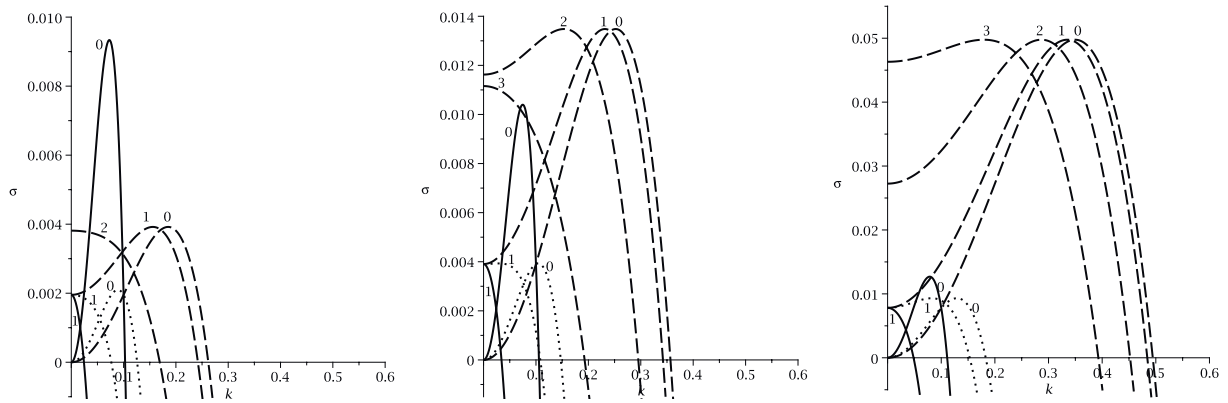

FIG. 5: σ vs. k; Bi = 0.1 and δ = 10. d/Q_C = 5. (a) Ma = 10, (b) Ma = 20, (c) Ma = 40. Solid Cr = 0.001, dotted Cr = 0.01, dashed Cr = 0.1; m = 0, 1, 2, 3

These results show that it is not possible, from the linear calculations, to determine which mode with $k_{max} > 0$ will prevail after the instability evolves in time. This conclusion can also be obtained from the paper by Moctezuma-Sánchez and Dávalos-Orozco (2015) when viscoelastic effects are neglected. However, here more detailed research was done of the linear stability equation which has the additional effects of the thermal conductivity and thickness of the wall. The goal of the analysis presented in the next section is to find out the parameter regions where the axial mode $m = 0$ and the first azimuthal mode can prevail from the nonlinear point of view.

3. SIDEBAND INSTABILITY

This section is devoted to investigating the sideband instability of the axial mode $m = 0$ into the azimuthal mode $m = 1$. To this end, Eq. (2) is scaled using $\xi = \sqrt{\text{Cr}}$. Thus, the following scalings are used: $z \to z/\xi$, $\delta \to a/\xi$, and $t \to 3t/\xi^2$. In this way, Eq. (2) was scaled into the following.

$$h_t + \nabla_\perp \cdot \left[h^3 \nabla_\perp \left(\frac{1}{a^2} h + \nabla_\perp^2 h \right) \right] + \frac{3}{2} \text{MaBi} \nabla_\perp \cdot \left\{ \frac{h^2}{\left[1 + \text{Bi} h + \text{Bi}(d/Q_C) \right]^2} \nabla_\perp h \right\} = 0. \tag{12}$$

Accordingly, the free surface deformation is expanded as

$$h = 1 + H(z, y, t). \tag{13}$$

Now, for $m = 1$ and $m = -1$, the free surface perturbation height H is expanded in normal modes as (Cheng and Chang, 1992)

$$\begin{aligned} H = {} & A_1 e^{ikz} + A_{1+\eta} e^{i(kz+\theta)} + A_{1-\eta} e^{i(kz-\theta)} + A_{c1} e^{-ikz} + A_{c1+\eta} e^{-i(kz+\theta)} + A_{c1-\eta} e^{-i(kz-\theta)} \\ & + A_2 e^{i2kz} + A_{2+\eta} e^{i(2kz+\theta)} + A_{2-\eta} e^{i(2kz-\theta)} + A_{c2} e^{-i2kz} + A_{c2+\eta} e^{-i(2kz+\theta)} + A_{c2-\eta} e^{-i(2kz-\theta)} \end{aligned} \tag{14}$$

where $A_{1+\eta}$ and $A_{1-\eta}$ are the time dependent amplitudes of the positive and negative sideband, respectively. The $A_{c1+\eta}$ and $A_{c1-\eta}$ are their corresponding complex conjugate time-dependent amplitudes. A similar definition is given to amplitudes with subindex 2. Then, the following set of nonlinear coupled ordinary differential equations is found.

$$\frac{dA_1}{dt} = \lambda_1 A_1 + \lambda_{1a} A_{c1} A_2 + \lambda_{1b} A_{c1-\eta} A_{2-\eta} + \lambda_{1c} A_{c1+\eta} A_{2+\eta} + \ldots, \tag{15}$$

$$\frac{dA_{1+\eta}}{dt} = \lambda_{1+\eta} A_{1+\eta} + \lambda_{1+\eta a} A_{c1-\eta} A_2 + \lambda_{1+\eta b} A_{c1} A_{2+\eta} + \ldots, \tag{16}$$

$$\frac{dA_{1-\eta}}{dt} = \lambda_{1-\eta}A_{1-\eta} + \lambda_{1-\eta a}A_{c1+\eta}A_2 + \lambda_{1-\eta b}A_{c1}A_{2-\eta} + \ldots, \tag{17}$$

$$\frac{dA_2}{dt} = \lambda_2 A_2 + \lambda_{2a}A_1^2 + \lambda_{2b}A_{1+\eta}A_{1-\eta} + \ldots, \tag{18}$$

$$\frac{dA_{2+\eta}}{dt} = \lambda_{2+\eta}A_{2+\eta} + \lambda_{2+\eta a}A_1A_{1+\eta} + \ldots, \tag{19}$$

$$\frac{dA_{2-\eta}}{dt} = \lambda_{2-\eta}A_{2-\eta} + \lambda_{2-\eta a}A_1A_{1-\eta} + \ldots, \tag{20}$$

where the parameters are

$$\lambda_1 = k^2(\mu^2 - k^2),$$

$$\lambda_{1a} = 2\lambda_1 - 19k^4 + \frac{2k^2}{a^2}S(\mathrm{Bi}, d/Q_c),$$

$$\lambda_{1b} = \lambda_{1c} = \lambda_{1a} + \frac{3k^2}{a^2},$$

$$\lambda_{1+\eta} = \lambda_{1-\eta} = \lambda_1 + \frac{1}{a^2}\left(\mu^2 - \frac{1}{a^2}\right) - 2\frac{k^2}{a^2},$$

$$\lambda_{1+\eta a} = \lambda_{1-\eta a} = 2\lambda_1 - k^4\left[21 - 2S(\mathrm{Bi}, d/Q_c)\right] - \frac{3}{a^4} + \frac{1}{a^2}\left[3 - S(\mathrm{Bi}, d/Q_c)\right]\left(k^2 + \frac{1}{a^2}\right),$$

$$\lambda_{1+\eta b} = \lambda_{1-\eta b} = \lambda_{1+\eta a} - \frac{18k^2}{a^2},$$

$$\lambda_2 = 4k^2(\mu^2 - 4k^2),$$

$$\lambda_{2a} = \lambda_2 S(\mathrm{Bi}, d/Q_c) + 2k^2\left(5k^2 + \frac{1}{a^2}\right) + 4k^2\left[1 - S(\mathrm{Bi}, d/Q_c)\right]\left(\frac{1}{a^2} - 4k^2\right),$$

$$\lambda_{2b} = 2\lambda_{2a} - \frac{12k^2}{a^2},$$

$$\lambda_{2+\eta} = \lambda_{2-\eta} = \lambda_2 + \frac{1}{a^2}\left(\mu^2 - \frac{1}{a^2}\right) - 8\frac{k^2}{a^2},$$

$$\lambda_{2+\eta a} = \lambda_{2-\eta a} = 2\left(\frac{1}{a^2} - \mu^2\right)S(\mathrm{Bi}, d/Q_c)\left(4k^2 + \frac{1}{a^2}\right) + 3k^2\left(4k^2 - \frac{1}{a^2}\right).$$

Here, $S(\mathrm{Bi}, d/Q_C) = 1 - \mathrm{Bi}/den$ and $den = 1 + \mathrm{Bi}(1 + d/Q_C)$. As will be seen presently, the following,

$$\mu^2 = \frac{1}{a^2} + \frac{3}{2}\frac{\mathrm{MaBi}}{\left[1 + \mathrm{Bi} + \mathrm{Bi}(d/Q_C)\right]^2},$$

is a very important parameter in the nonlinear problem.

It is assumed that the modes A_2, $A_{2+\eta}$, and $A_{2-\eta}$ are stable and $\lambda_2 < 0$ and $\lambda_{2+\eta} < 0$. Use is made of the slaved modes,

$$A_2 = C_1\lambda_{2a}A_1^2, \tag{21}$$

$$A_{2+\eta} = C_2\lambda_{2+\eta a}A_1A_{1+\eta}, \tag{22}$$

where $C_1 = 1/(-\lambda_2)$ and $C_2 = 1/(-\lambda_{2+\eta})$. There is an equation similar to Eq. (22), with the same coefficients, for $A_{2-\eta}$. Substitution of Eq. (21) into Eq. (15), neglecting higher-order terms, leads to the next equation satisfied by the axisymmetric mode (when $A_{1+\eta} = A_{1-\eta} = 0$).

$$\frac{dA_1}{dt} \sim \lambda_1 A_1 + C_1\lambda_{1a}\lambda_{2a}A_1 \mid A_1 \mid^2. \tag{23}$$

Equations (16) and (17) of $A_{1+\eta}$ and $A_{1-\eta}$ are linearized around the criticality of Eq. (23). That is,

$$| A_1 |^2 = -\frac{\lambda_1}{C_1 \lambda_{1a} \lambda_{2a}}. \tag{24}$$

The resulting coupled linear equations are

$$\frac{dA_{1+\eta}}{dt} = \lambda_{1+\eta} A_{1+\eta} - \frac{C_2}{C_1} \frac{\lambda_1 \lambda_{1+\eta b} \lambda_{2+\eta a}}{\lambda_{1a} \lambda_{2a}} A_{1+\eta} - \frac{\lambda_1 \lambda_{1+\eta a}}{\lambda_{1a}} A_{c1-\eta}, \tag{25}$$

$$\frac{dA_{1-\eta}}{dt} = \lambda_{1+\eta} A_{1-\eta} - \frac{C_2}{C_1} \frac{\lambda_1 \lambda_{1+\eta b} \lambda_{2+\eta a}}{\lambda_{1a} \lambda_{2a}} A_{1-\eta} - \frac{\lambda_1 \lambda_{1+\eta a}}{\lambda_{1a}} A_{c1+\eta}. \tag{26}$$

As can be seen, all these equations follow the procedure proposed by Cheng and Chang (1992). However, in the present problem, the definitions of $\lambda_{1+\eta}$ and $\lambda_{2+\eta}$ differ from those of Cheng and Chang and consequently dissimilar results are expected. The Jacobian J of the system of Eqs. (25) and (26) is

$$J = \begin{pmatrix} \lambda_{1+\eta} - \dfrac{C_2}{C_1} \dfrac{\lambda_1 \lambda_{1+\eta b} \lambda_{2+\eta a}}{\lambda_{1a} \lambda_{2a}} & -\dfrac{\lambda_1 \lambda_{1+\eta a}}{\lambda_{1a}} \\ -\dfrac{\lambda_1 \lambda_{1+\eta a}}{\lambda_{1a}} & \lambda_{1+\eta} - \dfrac{C_2}{C_1} \dfrac{\lambda_1 \lambda_{1+\eta b} \lambda_{2+\eta a}}{\lambda_{1a} \lambda_{2a}} \end{pmatrix}. \tag{27}$$

In general, from the Jacobian the conditions for stability are that the determinant $det(J) > 0$ and the trace $Tr(J) < 0$. If the discriminant of the eigenvalue solutions $(Tr(J))^2 - 4det(J)$ is positive the solution is stationary, if it is negative the solution is oscillatory. It can be shown that, due to the structure of J, the discriminant in our problem is $4\,(\lambda_1 \lambda_{1+\eta a}/\lambda_{1a})^2 > 0$ and the solutions are stationary [see also Cheng and Chang (1992)].

A number of critical values for μ^2 are calculated in the problem of the present paper. When the determinant of J is zero, four roots are found,

$$\lambda_{1+\eta} - \frac{C_2}{C_1} \frac{\lambda_1 \lambda_{1+\eta b} \lambda_{2+\eta a}}{\lambda_{1a} \lambda_{2a}} = \pm \frac{\lambda_1 \lambda_{1+\eta a}}{\lambda_{1a}}, \tag{28}$$

for each sign. When the trace of J is zero,

$$2 \left(\lambda_{1+\eta} - \frac{C_2}{C_1} \frac{\lambda_1 \lambda_{1+\eta b} \lambda_{2+\eta a}}{\lambda_{1a} \lambda_{2a}} \right) = 0 \tag{29}$$

four roots are found. Furthermore, as can be seen in Fig. 6 other curves are required: the curve of criticality of the axial mode [see Eq. (6) with $m = 0$] is $\mu_C^2 = k^2$ (solid), the curve of maximum growth rate of the axial mode [see Eq. (8) with $m = 0$] is $\mu_{max}^2 = 2k^2$ (dash-dotted), the curve below which the approximations of the nonlinear problem are valid is $\mu_{\lambda_2=0}^2 = 4k^2$ of $\lambda_2 = 0$ (large dashed), and the curve above which the first azimuthal mode [see Eq. (6) with $m = 1$] is unstable is $\mu_{C\mu=1}^2 = 2/a^2 + k^2$ (small dotted). Note that, except for the last one, these curves are independent of the radius of the cylinder; that is, they are the same in all Figs. 6(a)–6(c). Besides, they do not depend on the parameters group S(Bi, d/Q_c) which appears in some of the λ coefficients in Eqs. (15)–(20). Even more, under the present approximation, the valid solutions are confined between the curves $\mu_C^2 \leq \mu^2 \leq \mu_{\lambda_2=0}^2$, which do not change with the radius a and the other nondimensional parameters. These curves are presented in Fig. 6 for three different magnitudes of the radius a = 3, 5, and 10. On the contrary, the following curves depend on a and S(Bi, d/Q_c). The curve μ_E^2 is the lowest root found for the critical Eckhaus instability (dashed curve). This was calculated numerically using the method of Tuckerman and Barkley (1990). In the range $\mu_C^2 \leq \mu^2 \leq \mu_E^2$ the axial mode $m = 0$ is unstable. For $\mu^2 > \mu_E^2$ the axial mode is nonlinear stable. As can be seen in Fig. 6, the Eckhaus critical (lower dashed) curve μ_E^2 is very close to the critical curve of linear stability μ_C^2. Therefore, the axial mode is nonlinearly stabilized almost immediately for $\mu^2 \geq \mu_C^2$. Notice also the interesting result that the Eckhaus curve has a small region below the curve μ_C^2 for all the radii used in the paper. This suggests the possibility of subcritical instability in

that wave number range. For the results presented in Figs. 6 and 7, the magnitude $S(\mathrm{Bi}, d/Q_C)$ = 0.93 was selected. This corresponds to Bi = 0.1 and d/Q_C = 3.35.

Other important curves shown in Fig. 6 are those corresponding to the valid roots (for $\lambda_2 < 0$ or below $\mu^2_{\lambda_2=0}$) of the determinant of the Jacobian J [Eqs. (27) and (28)] with the plus sign μ^2_δ (below, large dotted) and $\mu^2_{\delta\delta}$ (above, large dotted). Above the dotted line $\mu^2_{Cm=1}$ and inside the range $\mu^2_\delta \leq \mu^2 \leq \mu^2_{\delta\delta}$ the axial mode $m = 0$ is unstable to the first azimuthal mode $m = 1$. This is the range of interest and the goal of the present paper. Clearly from Fig. 6(a), for small radius the required magnitudes of the wave number and μ^2 to destabilize the axial mode against $m = 1$ are very large. There are other roots of the determinant which are important but that are not drawn for the sake of presentation. They are the valid roots of the determinant with a minus sign [Eq. (28)] and the valid roots of the trace of the Jacobian J [Eq. (29)]. All these curves are plotted in Fig. 7 using an implicit plot command of the package Maple. For the sake of presentation some curves shown in Fig. 6 are not given in Fig. 7. It is interesting that all those valid curves are located inside the range $\mu^2_\delta \leq \mu^2 \leq \mu^2_{\delta\delta}$ (see Fig. 7). The roots of the determinant of J with minus sign [Eq. (28)] correspond to the dash-dotted curves and the roots of the trace [Eq. (29)] correspond to the dashed curves. Here it is important to point out that the lower branch of the valid roots of the determinant (plus and minus

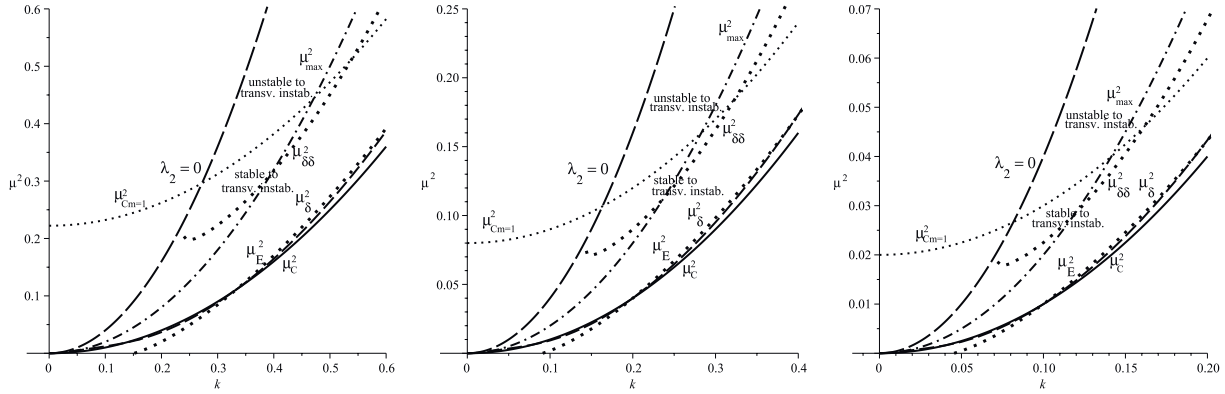

FIG. 6: μ^2 vs. k; a = Crδ; (a) a = 3, (b) a = 5, (c) a = 10

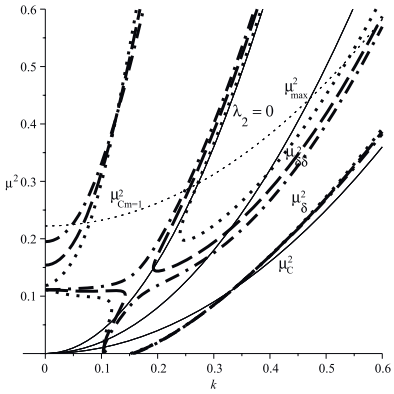

FIG. 7: Typical behavior of the roots of the determinant [Eq. (28)] and the trace [Eq. (29)] of the Jacobian matrix J [Eq. (27)]. Sample for a = 3. Valid (below curve of $\lambda_2 = 0$) and invalid (above curve of $\lambda_2 = 0$) roots of the determinant of the Jacobian J using the positive sign (large dotted lines), using the negative sign (dash-dotted lines), and the zeros of the trace (dashed lines) of the Jacobian J. Notice that the three lower branches almost superpose to each other and they appear as one curve which is still named μ^2_δ. Azimuthal modes are able to appear above the dotted line $\mu^2_{Cm=1}$. Furthermore, above μ^2_δ the axial mode $m = 0$ is unstable against mode $m = 1$, which becomes the most unstable one.

signs) and that of the trace are extremely close to each other and superpose in the graph of Fig. 7 in almost the same curve μ^2_δ. All those curves stay above μ^2_E after crossing the curve μ^2_C. Therefore, it is concluded that the axial mode $m = 0$ stabilizes above μ^2_E but with a slight increase of μ^2 it can be unstable to the first azimuthal mode $m = \pm 1$ above the curve μ^2_δ. However, as can be observed in Fig. 6, this mode is not unstable below $\mu^2_{Cm=1}$. Then, a large increase of μ is required to destabilize the first azimuthal mode, as shown by the dotted curve of $\mu^2_{Cm=1}$.

It is interesting that in Figs. 6(a)–6(c), mode $m = \pm 1$ destabilizes even for a $\mu^2 < \mu^2_{max}$, the maximum of the axial mode. This is in contrast with the results of Cheng and Chang (1992) for isothermal instability in the presence of gravity. Besides, the effect of the increase of a is to reduce the region of μ^2 where the axial mode is stable. In other words, the increase of a = Crδ widens the area of appearance of azimuthal modes. Notice that in the limit $a \to \infty$ (see also the definition of μ^2) the problem is reduced to that of the thermocapillary instability of a film on a flat thick plate with finite thermal conductivity. Moreover, when Ma = 0 the results describe the instability of the isothermal problem, only due to surface tension instability.

With all these roots, as shown in Fig. 7, it is possible to describe the kind of critical points of the solutions of Eqs. (25) and (26). The following notation is used. The valid roots of the determinant with minus sign [Eq. (28)] are μ^2_{-L} (lower branch) and μ^2_{-U} (upper branch); the roots of the trace [Eq. (29)] are μ^2_{traceL} (lower branch) and μ^2_{traceU} (upper branch). Then, for $\mu^2 < \mu^2_\delta$ (μ^2_{-L}, μ^2_{traceL}), [$Tr(J) < 0$, $det(J) > 0$] the critical point is a stable node. For μ^2_δ (μ^2_{-L}, μ^2_{traceL}) $< \mu^2 < \mu^2_{-U}$ [$Tr(J) > 0$, $det(J) > 0$] the critical point is an unstable node. For $\mu^2_{-U} < \mu^2 < \mu^2_{traceU}$ [$Tr(J) > 0$, $det(J) < 0$] the critical point is a saddle point. For $\mu^2_{traceU} < \mu^2 < \mu^2_{\delta\delta}$ [$Tr(J) < 0$, $det(J) < 0$] the critical point is a saddle point, and for $\mu^2_{\delta\delta} < \mu^2 < 4k^2$ ($\lambda_2 = 0$) [$Tr(J) < 0$, $det(J) > 0$] the critical point is a stable node.

4. CONCLUSIONS

The goal of this paper was to solve the indeterminacy found, under the present approximation, in the linear problem for the azimuthal instability of a thin film coating the outside of a cylinder with a thick wall and finite thermal conductivity. Use is made of the full evolution equation with a scaling in the coordinates and time by means of Cr. Even with this full nonlinear equation, it was possible to apply, in a more complex way, the theory by Cheng and Chang (1992) for the first time in a thermocapillary problem on a cylinder. In this way, by means of the sideband instability, the regions where the axial mode prevails and the area where it is unstable to the first azimuthal mode were determined. It was found that the radius of the cylinder plays the important role of exciting the instability of the azimuthal modes.

In fact, for a large enough wave number, the first azimuthal mode is able to appear below the maximum growth rate of the axial mode $m = 0$. This occurs for a wave number above the intersection of the curves $\mu^2_{Cm=1}$ and $\mu^2_{\delta\delta}$ where the axial mode is already unstable against $m = 1$. Both curves depend on a and therefore the intersection occurs for smaller k with the increase of a. At the same time, the magnitude of μ^2 required to destabilize $m = 1$ decreases with a.

A number of different critical magnitudes of μ^2 were found. With them it was possible to understand the characteristics of the critical points of the equations [Eqs. (25) and (26)] obtained from the normal mode expansion. The instability regions of the axial mode were located by means of these critcal points. It was shown that the axial mode is unstable against the first azimuthal mode only in the range $\mu^2_\delta < \mu^2 < \mu^2_{\delta\delta}$. The axial mode is stable against $m = 1$ for $\mu^2 < \mu^2_\delta$ and $\mu^2 > \mu^2_{\delta\delta}$. However, it is expected that in the range $\mu^2_{\delta\delta} < \mu^2 < \mu^2_{\lambda_2=0}$ (and for smaller wave numbers) it could be possible to find mode $m = 2$ as the most unstable one.

ACKNOWLEDGMENTS

The author would like to thank Alberto López, Alejandro Pompa, Cain González, Raúl Reyes, Ma. Teresa Vázquez, and Oralia Jiménez for technical support.

REFERENCES

Benney, D.J., Long Waves on Liquid Films, *J. Math. Phys.*, vol. **45**, nos. 1-4, pp. 150–155, 1966. DOI: 10.1002/sapm1966451150

Cheng, M.Q. and Chang, H.-C., Stability of Axisymmetric Waves on Liquid Films Flowing down a Vertical Column to Azimuthal and Streamwise Disturbances, *Chem. Eng. Commun.*, vol. **118**, no. 1, pp. 327–340, 1992. DOI: 10.1080/00986449208936101

Dávalos-Orozco, L.A., The Effect of the Thermal Conductivity and Thickness of the Wall on the Nonlinear Instability of a Thin Film Flowing down an Incline, *Int. J. Nonlinear Mech.*, vol. **47**, no. 4, pp. 1–7, 2012. DOI: j.ijnonlinmec.2012.02.008

Dávalos-Orozco, L.A., Nonlinear Instability of a Thin Film Flowing down a Smoothly Deformed Thick Wall of Finite Thermal Conductivity, *Interf. Phenom. Heat Transf.*, vol. **2**, no. 1, pp. 55–74, 2014. DOI: 10.1615/InterfacPhenomHeatTransfer.2014010400

Dávalos-Orozco, L.A., Non-Linear Instability of a Thin Film Flowing down a Cooled Wavy Thick Wall of Finite Thermal Conductivity, *Phys. Lett. A*, vol. **379**, nos. 12-13, pp. 962–967, 2015. DOI: 10.1016/j.physleta.2015.01.018

Dávalos-Orozco, L.A., Thermal Marangoni Instability of a Thin Film Flowing down a Thick Wall Deformed in the Backside, *Phys. Fluids*, vol. **28**, no. 5, p. 054103, 2016. DOI: 10.1063/1.4948253

Dávalos-Orozco, L.A. and Ruiz-Chavarría, G., Hydrodynamic Instability of a Fluid Layer Flowing down a Rotating Cylinder, *Phys. Fluids A*, vol. **5**, no. 10, pp. 2390–2404, 1993. DOI: 10.1063/1.858753

Dávalos-Orozco, L.A. and You, X., Three-Dimensional Instability of a Liquid Layer Flowing down a Heated Vertical Cylinder, *Phys. Fluids*, vol. **12**, no. 9, pp. 2198–2209, 2000. DOI: 10.1063/1.1286594

Dijkstra, H.A., The Coupling of Marangoni and Capillary Instabilities in an Annular Thread of Liquid, *J. Colloid Interf. Sci.*, vol. **136**, no. 1, pp. 151–159, 1990. DOI: 10.1016/0021-9797(90)90085-3

Frenkel, A.L., Babchin, A.J., Levich, B.G., Shlang, T., and Sivashinsky, G.I., Annular Flows Can Keep Unstable Films from Breakup: Nonlinear Saturation of Capillary Instability, *J. Colloid Interf. Sci.*, vol. **115**, no. 1, pp. 225–233, 1987. DOI: 10.1016/0021-9797(87)90027-0

Frenkel, A.L., (1993), On Evolution Equations for Thin Films Flowing down Solid Surfaces, *Phys. Fluids A*, vol. **5**, no. 10, pp. 2342–2347, 1993. DOI: doi.org/10.1063/1.858895

Krishnamoorthy, S., Ramaswamy, B., and Joo, S.W., Spontaneous Rupture of Thin Liquid Films due to Thermocapillarity: A Full-Scale Direct Numerical Simulation, *Phys. Fluids*, vol. **7**, no. 9, pp. 2291–2293, 1995. DOI: 10.1063/1.868478

Moctezuma-Sáchez, M. and Dávalos-Orozco, L.A., Linear Three Dimensional Instability of Viscoelastic Fluid Layers Flowing down Cylindrical Walls, *Micrograv. Sci. Technol.*, vol. **20**, pp. 161–164, 2008. DOI: 10.1063/1.858895

Moctezuma-Sáchez, M. and Dávalos-Orozco, L.A., Azimuthal Instability Modes in a Viscoelastic Liquid Layer Flowing down a Heated Cylinder, *Int. J. Heat Mass Transf.*, vol. **90**, pp. 15–25, 2015. DOI: j.ijheatmasstransfer.2015.06.035

Ruiz-Chavarría, G. and Dávalos-Orozco, L.A., Stability of a Liquid Film Flowing down a Rotating Cylinder Subject to Azimuthal Disturbances, *J. Phys. II*, vol. **6**, no. 8, pp. 1219–1227, 1996. DOI: 10.1051/jp2:1996126

Ruiz-Chavarría, G. and Dávalos-Orozco, L.A., Azimuthal and Streamwise Disturbances in a Fluid Layer Flowing down a Rotating Cylinder, *Phys. Fluids*, vol. **9**, no. 10, pp. 2899–2908, 1997. DOI: 10.1063/1.869402

Shlang, T. and Sivashinsky, G.I., Irregular Flow of a Liquid Film down a Vertical Column, *J. Phys. (Paris)*, vol. **43**, no. 3, pp. 459–466, 1982. DOI: 10.1051/jphys:01982004303045900

Tuckerman, L.S. and Barkley, D., Bifurcation Analysis of the Eckhaus Instability, *Phys. D: Nonlin. Phenom.*, vol. **46**, no. 1, pp. 57–86, 1990. DOI: 10.1016/0167-2789(90)90113-4